THE JOURNAL OF CHEMICAL PHYSICS **133**, 224502 (2010)

Chiral symmetry breaking in a microscopic model with asymmetric autocatalysis and inhibition

Harold W. Hatch,[1] Frank H. Stillinger,[2] and Pablo G. Debenedetti[1,a)]
[1]*Department of Chemical and Biological Engineering, Princeton University, Princeton, New Jersey 08544, USA*
[2]*Department of Chemistry, Princeton University, Princeton, New Jersey 08544, USA*

(Received 19 July 2010; accepted 17 October 2010; published online 9 December 2010)

Asymmetric autocatalysis and inhibition have been proposed as key processes in the spontaneous emergence of chiral symmetry breaking in a prebiotic world. An elementary lattice model is formulated to simulate the kinetics of chiral symmetry breaking via autocatalysis and inhibition in a mixture of prochiral reactants, chiral products, and inert solvent. Starting from a chirally unbiased initial state, spontaneous symmetry breaking occurs in spite of equal *a priori* probability for creating either product enantiomer, and the coupled reaction–diffusion processes subsequently amplify the random early-stage symmetry breaking. The processes of reaction and diffusion are kinetically intertwined in a way leading to competition in the appearance of enantiomeric excess. An effective transition temperature can be identified below which spontaneous symmetry breaking appears. In the absence of inhibition, reactions are predominantly autocatalytic under both reaction control (fast diffusion, slow reaction) or diffusion control (fast reaction, slow diffusion) conditions. In the presence of inhibition, simulations with different system sizes converge to the same transition temperature under reaction control conditions, and in this limit the reactions are predominantly nonautocatalytic. © *2010 American Institute of Physics*. [doi:10.1063/1.3511715]

I. INTRODUCTION

Chirality is an essential characteristic of life. Biological molecules are composed of subunits that exhibit only one of the two possible chiral forms. Nineteen of the 20 naturally-occurring amino acids are chiral, with exclusively the L-form found in proteins during translation in the ribosome. Most naturally occurring sugars are D-isomers, as exemplified by the ribose units in nucleic acids. Fundamental questions naturally arise about the origin of biological homochirality. According to one viewpoint, symmetry breaking is an intrinsic property of polymerizing systems composed of chiral units, and it arises from purely statistical considerations when the number of mathematically possible sequences exceeds the number of sequences that can actually be formed in a large but finite collection of polymerizing units.[1,2] It has been pointed out, however,[3] that prebiotic models of nonenzymatic polymerization require a source of homochirality in order to explain a primitive "RNA world" because in template-directed extension of D-RNA in a racemic solution, L-nucleotides act as chain terminators.[4] Thus, the investigation of possible physical mechanisms that can explain the origin of homochirality in a presumably racemic prebiotic environment constitutes an active area of current research.[3,5–7]

Both kinetic[8] and equilibrium processes may lead to spontaneous chiral amplification. One possible thermodynamic mechanism entails equilibrium phase behavior in a poor solvent,[9–14] and it involves the formation of both racemic and enantiopure crystals in equilibrium with a liquid phase enriched in one of the enantiomers. Interestingly, several proteinogenic amino acids exhibit such phase behavior in water.[10,12] This mechanism spontaneously amplifies an initial chiral imbalance but cannot create chiral asymmetry from racemic conditions. Molecular simulation of solid–fluid equilibrium in simple models of chiral molecules can shed light on the type of interactions that favor different solid phases.[15] Another mechanism entails attrition of an initially equilibrated saturated solution containing equal amounts of mirror enantiomorphic crystals, resulting in a single enantiomorphic crystal phase.[16–19] The interpretation of this phenomenon remains a subject of debate.[20–22]

A phenomenological kinetic scenario involving autocatalysis and inhibition, leading to chiral amplification starting from a small imbalance, was proposed many years ago.[23] Nearly half a century later, experimental proof of concept of the role of autocatalysis in asymmetric amplification from low enantiomeric excess catalyst was provided by Soai and coworkers.[24–26] A kinetic model that provides a simple explanation of the asymmetric amplification observed in the Soai reaction was provided by Blackmond and co-workers.[27] The Soai reaction remains the only reaction to our knowledge that yields high enantiomeric excess of catalyst product from low enantiomeric excess of catalyst reactants.[28]

Several studies have been conducted on the Soai reaction[27,29,30] and spontaneous asymmetric synthesis,[31,32] but the effects of diffusion and inhibition mechanisms on chiral symmetry breaking are not in general well understood. Few models include spatial degrees of freedom,[33,34] which is a prerequisite to investigating diffusion. Possible inhibition mechanisms that have been considered span the range from physical processes such as crystallization[35] to molecular interactions,[36] but there is no general framework for understanding the effect of the inhibition mechanism on

[a)]Author to whom correspondence should be addressed. Electronic mail: pdebene@princeton.edu.

chiral symmetry breaking. In this work, we formulate a simple microscopic model that includes diffusion, autocatalysis, and inhibition, and we investigate numerically the conditions leading to chiral symmetry breaking in the reaction products, starting from perfectly symmetric conditions.

In addition to the above-mentioned implications for the origin of life, chirality is also of considerable practical interest in pharmacology. Therapeutic compounds often must be synthesized with a particular chirality, and in extreme cases the mirror image may be harmful. A notable example is Thalidomide, whose (R)-enantiomer treats morning sickness, while the (S)-enantiomer causes birth defects.[37] In this case, dosing with an enantiopure drug may still cause birth defects because the two isomers interconvert *in vivo*. Another example is (S, S)-ethambutol, which is used in the treatment of tuberculosis, while the (R, R)-enantiomer shows no antimicrobial activity and the (R, S)-enantiomer possesses about one tenth of the activity of the (S, S) molecule.[38] All enantiomers possess the same toxicity, which necessitates the production of pure (S, S)-ethambutol. These examples illustrate the importance for the pharmaceutical industry of research aimed at identifying ways to spontaneously amplify one chiral form over another.

In Sec. II, we introduce a simple lattice model with autocatalysis and inhibition that allows the possibility of assessing quantitatively the effects of reaction and diffusion rates, and inhibition mechanisms, on spontaneous chiral symmetry breaking. To our knowledge, this is the first model with molecularly explicit chirality, spatial degrees of freedom, autocatalysis, and inhibition that exhibits symmetry breaking. It is important to note that this model provides a minimal description that nevertheless captures the underlying chemistry and physics. The fact that the model is two-dimensional is purely incidental, but allows for easy visualization of the kinetic processes involved. The numerical simulation method used to investigate the model's behavior is then discussed, followed by a presentation of the results, and discussion. Finally, a summary and concluding remarks about future lines of inquiry are presented.

II. MODEL

Two reactive species, A and B, initially inhabit the sites of a two-dimensional square lattice. Prochiral A particles, that is to say, particles that can be converted from achiral to chiral in a single reaction, occupy a single site, while prochiral B particles occupy a nearest-neighbor pair of sites. Multiple occupancy of a lattice site is forbidden. The unoccupied sites can be interpreted either as empty space or as residency sites for structureless and chemically inert solvent particles. These reactive species, A and B, will be subject to stochastic dynamics that cause translational diffusion by nearest neighbor jumps and, for multisite species, rotational diffusion by rotation about the centermost site(s); and these A and B reactants are also subject to irreversible chemical reactions that produce rigid chiral C enantiomers as shown in Fig. 1(a). Because the C enantiomers are confined to a two-dimensional lattice, no translation and/or rotation can interconvert them; to do so would require lifting the rigid bent C up into a third dimension, flipping it over, and then returning it to the two-dimensional lattice.

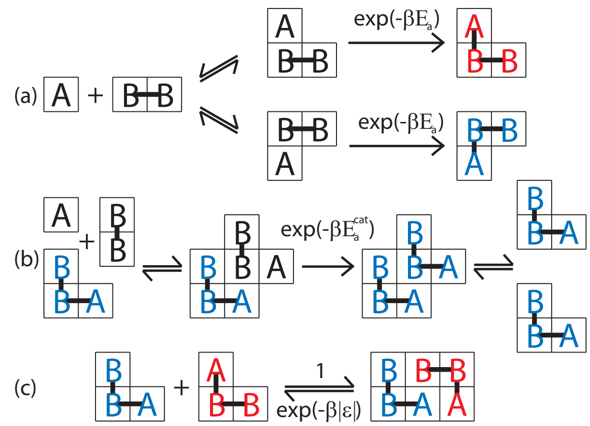

FIG. 1. Kinetic transitions in the model. Enantiomers with chirality are colored red and blue for clarity and are distinguishable by the relative orientation of the bonded A and B particles. (a) Nonlinear clusters of non-chiral A and B particles are stochastically formed by diffusion, which may stochastically and irreversibly react with a rate $\exp(-\beta E_a)$ to form rigid C enantiomers, depicted by a chemical bond between A and B particles, where E_a is the activation energy, β is $1/k_BT$, T is the temperature, and k_B is the Boltzmann constant. Once formed, a rigid C enantiomer may translate and rotate diffusively in two dimensions but cannot invert to the other C enantiomer. (b) C enantiomers may autocatalyze the formation of other C enantiomers with the same chirality at a rate of $\exp(-\beta E_a^{cat})$ when a nonlinear cluster of A and B particles forms in the cleft of a C enantiomer, where $E_a > E_a^{cat} > 0$. (c) Two C enantiomers of differing chirality may form inactive dimers by binding to each other's clefts with strength $\epsilon \leq 0$, thereby mutually inhibiting their autocatalysis mechanism. Only the relative orientation of particles is important and only one special case of the four possible orientations is shown in parts (a), (b), and (c).

Let $\exp(-\beta E_a)$ be the reaction rate for a nonlinear cluster of nonchiral A and B particles to form a C enantiomer, where E_a is the activation energy, β is $1/k_BT$, T is the temperature, k_B is the Boltzmann constant, and the pre-exponential factor has been set to unity. The activation energy, $E_a > 0$, applies regardless of the orientation or chirality of the potential product C enantiomer. With one important exception, the activation energy, E_a, applies to bent clusters, regardless of the composition (A, B, C, empty) of the neighboring sites. The exception involves autocatalysis, with a reaction rate $\exp(-\beta E_a^{cat})$, where E_a^{cat} is the activation energy of the autocatalytic reaction, subject to the inequality $E_a > E_a^{cat} > 0$. The autocatalytic activation energy, E_a^{cat} applies when an unreacted nonlinear A, B cluster resides in the cleft of a C enantiomer of the same chirality, as illustrated in Fig. 1(b).

The model as described above possesses an autocatalytic mechanism, but no inhibition. However, if two C enantiomers of differing chirality were to bind to each other's cleft forming an inactive dimer, they would no longer participate in the autocatalytic mechanism. If the C enantiomers are present in unequal amounts, the formation of an inactive dimer would cause the minority catalyst population to decrease by a fraction greater than that for the majority. Thus, dimer binding of C enantiomers represents specific mutual antagonism.[23,28] Let $\epsilon \leq 0$ be the favorable dimer binding energy when two C

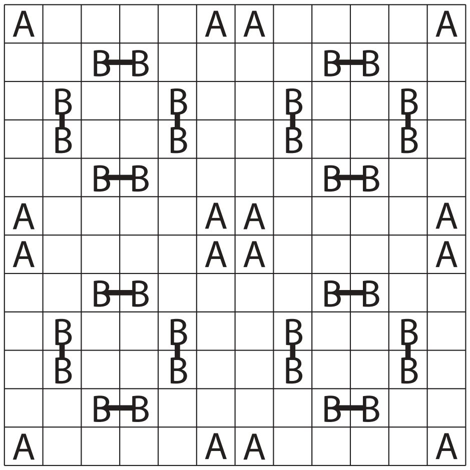

FIG. 2. Example of four 6 × 6 lattice unit cells at a coverage fraction of $\phi = 1/3$ that, by periodic replication, is used to generate initial configurations for larger systems. Importantly, the configuration contains no initial bias for the formation of one enantiomer over another, on account of its symmetry.

enantiomers of opposite chirality reside in each other's cleft, as illustrated in Fig. 1(c).

III. METHODS

Numerical solution of the model is possible with a simple rejection kinetic Monte Carlo algorithm,[39] which randomly attempts and accepts transitions with rules described in what follows. A particle is randomly selected. If that particle is of type A or B, a reactive or diffusive transition is attempted with equal probability. If that particle is of type C, a diffusive transition is attempted. Reactive transitions are accepted with probability $\omega_r = \exp(-\beta \Delta E)$, where $\Delta E = +\infty$ if the selected particle does not have a neighboring reactant in the correct configuration, E_a^{cat} if an autocatalytic configuration produces C enantiomers of the same chirality, and E_a otherwise where $E_a > E_a^{cat} > 0$. Diffusive transitions are accepted with probability $\omega_d = \exp(-\beta \Delta E)$, where $\Delta E = +\infty$ if the attempt leads to particle overlap, $|\epsilon|$ if two C enantiomers of the opposite chirality both reside within the other's cleft, and zero otherwise. When $|\epsilon|$ is large, inactive dimers are likely to remain stationary for the remainder of the simulation. Diffusion takes place in a good solvent such that all interaction energies are equal, except when two C enantiomers of opposite chirality form an inactive dimer as illustrated in Fig. 1(c). Solvent is implicitly assumed to flow out of the way of A, B, and C diffusive jumps as necessary. Time, t is incremented after each attempt by $\Delta t = \tau/N$, where N is the total number of A, B, and C particles and τ is the average interval over which each particle is excited once (i.e., visited) by an implicit heat bath.

The initial configuration contains no bias for the formation of one enantiomer over another, on account of its symmetry, as exemplified in Fig. 2. A simulation is conducted on a finite two-dimensional square lattice of size n_x by n_y, $n_x = n_y$, with a lattice spacing of l and with periodic boundary conditions. Our numerical simulations have utilized both $n_x = 36$ and $n_x = 90$. Irreversible reactions lead to a decrease in the amount of A and B present, and a simulation is completed when the reactant A diminishes in mole fraction to a preset value x_A. The time-dependent discrete probability distribution function of the fraction present of a given enantiomer, f, and the corresponding distribution of enantiomeric excess, ee are approximated by averaging over a large number of equivalent simulations, $n_s \geq 10^4$. There is no need to specify the enantiomer implied in the fraction, f, because the model treats both chiral forms symmetrically, which guarantees symmetric probability distribution functions for a large ensemble of simulations. The fraction, f, and the enantiomeric excess, ee, are related by the formula $ee = |2f - 1|$. Because these are discrete probability distribution functions, the resolution is determined by the number of enantiomers present.

The sample skewness of the enantiomeric excess, $g_1(ee)$, is a convenient parameter to characterize the extent of symmetry breaking and is defined as

$$g_1(ee) = \frac{\sqrt{n_s(n_s-1)}}{n_s - 2} \frac{m_3}{m_2^{3/2}}, \tag{1}$$

where m_2 and m_3 are the second and third central moments, respectively, of the distribution of the enantiomeric excess.[40]

The Einstein expression is used to compute the diffusion coefficient, D_i, for a given species, i, in the absence of reaction and is given by

$$D_i = \lim_{t\to\infty} \frac{\langle [\mathbf{r}_i(t'+t) - \mathbf{r}_i(t')]^2 \rangle_{t'}}{4t}, \tag{2}$$

where $\mathbf{r}_i(t)$ is the position of a particle of species i at time t and $\langle \cdots \rangle_{t'}$ is an average over all particles of species i and time origins, t'.

IV. RESULTS AND DISCUSSION

Simulations at various coverage fractions were conducted in the absence of reaction to study the composition dependence of diffusion coefficients. The diffusion coefficients in the absence of reaction for the pure components, D_i, equimolar A, B mixtures, D_i^{AB} and equimolar A, B, C mixtures, D_i^{ABC} for various coverage fractions, ϕ, are shown in Fig. 3. These results are not needed as input to the reactive simulations, but were, rather, conducted as a preliminary investigation of diffusive motion in this model. The diffusion coefficients at infinite dilution, in units of l^2/τ, are 1/4 3/16 and 1/6 for A, B, and C, respectively. Infinite dilution diffusion coefficients were also derived by means of the master equation and agree with simulation results. As the coverage fraction is increased, species with more sites experience greater steric hindrance to displacement [Fig. 3(a)]. At the same coverage fraction, A is more mobile in an equimolar A, B mixture than in pure A, while B is less mobile in an equimolar A, B mixture than in pure B, as shown in Fig. 3(b). This trend is found to be monotonic with coverage fraction. Equimolar A, B, C mixtures, however, possess nonmonotonic dependence on coverage fraction, as shown in Fig. 3(c). For low coverage fractions, A is more mobile in equimolar A, B, C mixtures than in pure A, while C is less mobile. At sufficiently high coverage fractions, however, this trend reverses such that A is less mobile in equimolar A, B, C mixtures than

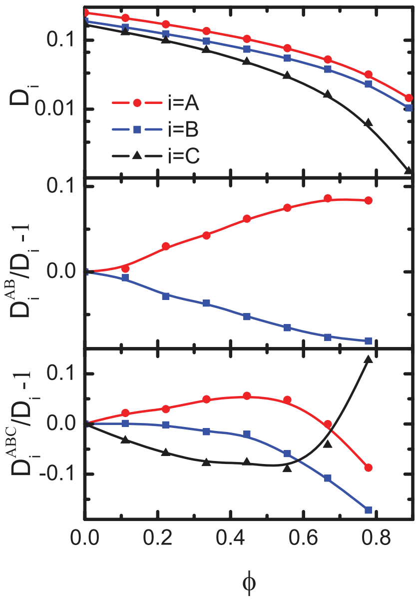

FIG. 3. (a) Top. Pure component diffusion coefficients, D_i, of species i in the absence of reaction, as a function of the coverage fraction ϕ. Diffusion coefficients are reported in units of l^2/τ. (b) Middle. Normalized difference between equimolar A, B mixture diffusion coefficients, D_i^{AB}, and the corresponding pure component quantities. (c) Bottom. Normalized differences between equimolar A, B, C mixture diffusion coefficients, D_i^{ABC}, and the corresponding pure component quantities. All simulations containing C enantiomers are racemic. No reactions are attempted, the simulation is terminated at $t/\tau = 100$; $\epsilon = 0$, $n_x = n_y = 36$, and the mean squared displacement is averaged over 1000 independent trajectories. The statistical error, smaller than symbols, is of the order of $10^{-3}\ l^2/\tau$.

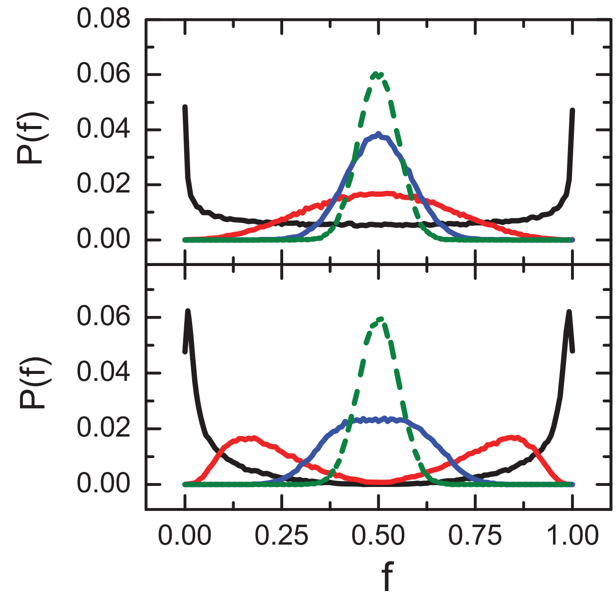

FIG. 4. (a) Top. Discrete probability distribution function, $P(f)$, of the fraction of a given enantiomer, f, averaged over n_s simulations, is shown for $E_a^{cat}/E_a = 0$, $\epsilon/E_a = 0$, $n_x = n_y = 36$, $n_s = 10^5$, $\phi = 1/3$, and $x_A = 0.1$. Symmetry breaking occurs at $\beta E_a = 10$ (solid black line), while symmetry breaking does not occur at the higher temperatures $\beta E_a = 8$ (solid red line), $\beta E_a = 6$ (solid blue line) and $\beta E_a = 4$ (dashed green line). (b) Bottom. As above except $\epsilon/E_a = -10$. With inhibition, symmetry breaking occurs at $\beta E_a = 10$ and 8, where the bimodal distributions possess local maxima.

in pure A, while C is more mobile. Despite the simplicity of the lattice model, interesting phenomena occur as a function of coverage fraction and mixture composition which merit further study.

Simulations with reactions were conducted to study symmetry breaking. Discrete probability distribution functions, P, of both the fraction, f, and the enantiomeric excess, ee, are shown in Figs. 4 and 5, respectively. Symmetry breaking, evidenced by a bimodal probability distribution of f, is observed for sufficiently low temperatures. Under symmetry-broken conditions, there is a high probability that a simulation will lead to substantial enantiomeric excess, and a correspondingly small probability that a racemic mixture will result. The symmetry of $P(f)$ about $f = 0.5$ means that enantiomeric excess of either chiral product is equally probable when averaged over a large number of simulations.

Local maxima in the probability distribution functions arise as a result of inhibition. Consider Fig. 4. The probability distribution functions at $f = 1$ and 0 must be precisely equal with or without inhibition because when the system remains enantiopure, no inactive dimers may form and the simulations are equivalent. The probability at $f = 1/2$ when inhibition is present, however, is always less than in the absence of inhibition. Inhibition shifts the probability toward the extremes, while $P(0)$ and $P(1)$ are pinned at constant values, leading directly to local maxima.

When symmetry breaking occurs, $g_1(ee) < 0$, the tail of the distribution is larger on the left than the right, and the majority of values lie to the right of the mean. When symmetry breaking does not occur, $g_1(ee) > 0$. Thus, the skewness of the ee is a convenient parameter to quantify the extent of symmetry breaking. An important physical quantity is $\beta^* = 1/k_B T^*$, where T^* is the transition temperature at which $g_1(ee) = 0$. The skewness, $g_1(ee)$, is simply the normalized third central moment and is therefore zero for a symmetric probability distribution of the enantiomeric excess.

The overall behavior of the model system is summarized in Fig. 6, where all points lying above a given line represent

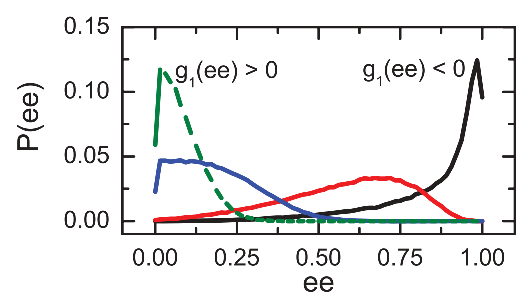

FIG. 5. Discrete probability distribution function, $P(ee)$, of the enantiomeric excess, ee, corresponding to the same set of simulations as shown in Fig. 4(b). Symmetry breaking occurs at $\beta E_a = 10$ (solid black line) and 8 (solid red line), in which case the skewness, $g_1(ee) < 0$. Symmetry breaking does not occur at the higher temperatures $\beta E_a = 6$ (solid blue line) and $\beta E_a = 4$ (dashed green line), when the skewness, $g_1(ee) > 0$. Thus, the skewness of the enantiomeric excess is a convenient parameter to quantify the extent of symmetry breaking. A transition from nonsymmetry broken states to symmetry broken states is defined to occur when the probability distribution function of enantiomeric excess is symmetric, in which case the skewness, $g_1(ee)$, or third central moment, is zero. The sudden downturn at $ee = 0$ is due to the discreteness of $P(ee)$, leading to half the expected probability with an odd number of possible outcomes.

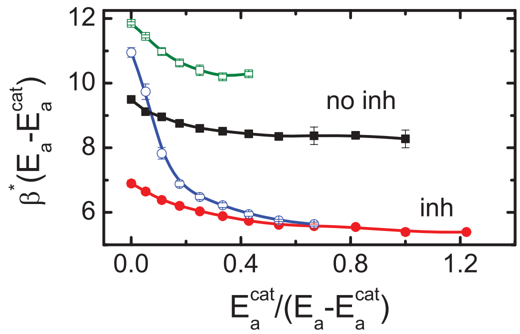

FIG. 6. Loci of β^*, where all points above a given line represent symmetry broken states. System sizes of $n_x = 36$ (solid circles and squares) and $n_x = 90$ (open circles and squares) were simulated with $\epsilon = 0$ (no inhibition; squares) and $\epsilon/E_a = -10^6$ (with inhibition; circles). $n_s = 10^4$, $\phi = 1/3$, and $x_A = 0.1$. For the three rightmost points on the black curve (solid squares), $n_s = 10^3$ due to slow simulation times.

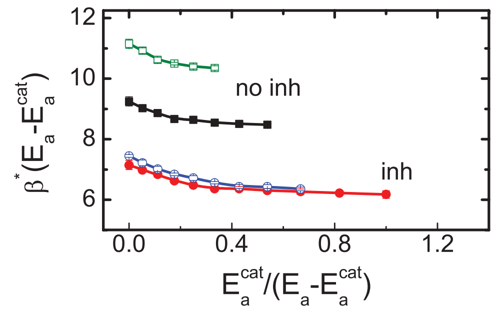

FIG. 8. Same as Fig. 6, except $\phi = 1/6$. Loci of β^*, where all points above a given line represent symmetry broken states. System sizes of $n_x = 36$ (solid circles and squares) and $n_x = 90$ (open circles and squares) were simulated with $\epsilon = 0$ (no inhibition; squares) and $\epsilon/E_a = -10^6$ (with inhibition; circles). $n_s = 10^4$, $\phi = 1/6$, and $x_A = 0.1$.

symmetry broken states corresponding to a particular choice of model parameters. As E_a^{cat} increases for a given $E_a - E_a^{cat}$, reactions become slower relative to diffusion, and the system is said to be under reaction control. The quantity β^* is found by successively incrementing βE_a by 0.1 and determining the $g_1(ee)$ average and standard deviations from five block averages of n_s simulations total. Figure 7 shows the fraction of the total number of reaction events that are noncatalytic for each β^* in Fig. 6. As summarized in Fig. 6, two fundamentally different forms of symmetry breaking can occur in the present model. With no favorable dimer binding energy, that is to say in the absence of an inhibition mechanism (curves marked no inh), symmetry breaking occurs by a predominantly autocatalytic route, favored by low temperatures (large β^*). The enantiomeric excess of the system then depends largely on the first noncatalytic reaction. With favorable inactive dimer binding energy, that is to say when an inhibition mechanism is present (curves marked inh), symmetry breaking may occur even when a majority of the reactions are nonautocatalytic. In this case, the transition temperature plateaus upon increasing the diffusion rate into the reaction-limited regime. In this regime, two different system sizes plateau to the same transition temperature, which suggests the attainment of a system-size independent transition temperature for sufficiently high diffusion rates, and favorable inactive dimer binding energy. Under diffusion control ($E_a^{cat} \rightarrow 0$ for a given $E_a - E_a^{cat}$), lower temperatures are needed in order for symmetry breaking to occur in progressively larger systems. In the absence of inhibition, the inverse relation between temperature and system size persists into the reaction control regime.

Figures 8 and 9 summarize the overall behavior of the model system for a coverage fraction, $\phi = 1/6$. For lower coverage fractions, simulations without inhibition are essentially equivalent to the higher coverage fraction simulations. In the presence of inhibition, however, the system-size dependence is appreciably reduced relative to $\phi = 1/3$ case (Fig. 6). Regions of diffusion control are expected to shrink with decreased coverage fraction because, as shown in Fig. 3, diffusion coefficients increase markedly with decreasing ϕ. Note that although the system sizes considered ($n_x = 36$ and 90) are the same in Fig. 8, the lower coverage fraction simulations have half the number of molecules, which promotes symmetry breaking. Initial configurations were generated by using the unit cells shown in Fig. 2, but evacuating columns of unit cells in alternating fashion. For example, particles in the two right-most unit cells in the 2×2 unit cell initial condition shown in Fig. 2 would be removed. For $n_x = 90$, half of the particles in the fifteenth column of unit cells were removed. Simulations were also

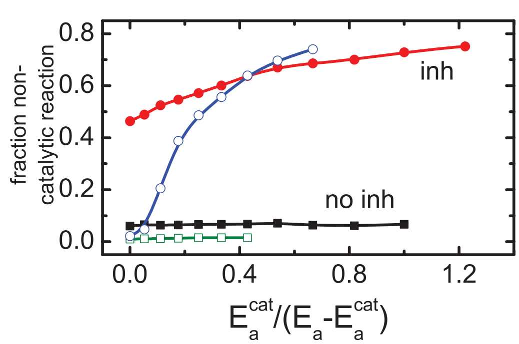

FIG. 7. Fraction of total number of reaction events that are noncatalytic, corresponding to each β^* in Fig. 6. System sizes of $n_x = 36$ (solid circles and squares) and $n_x = 90$ (open circles and squares) were simulated with $\epsilon = 0$ (no inhibition; squares) and $\epsilon/E_a = -10^6$ (with inhibition; circles). $n_s = 10^4$, $\phi = 1/3$, and $x_A = 0.1$.

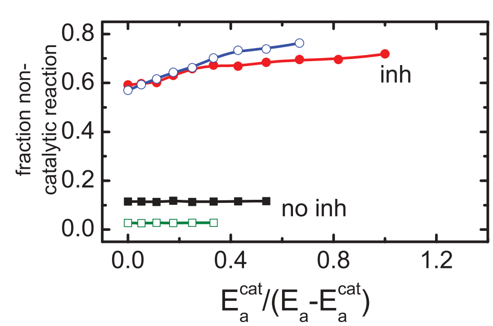

FIG. 9. Same as Fig. 7, except $\phi = 1/6$. Fraction of total number of reaction events that are noncatalytic, corresponding to each β^* in Fig. 8. System sizes of $n_x = 36$ (solid circles and squares) and $n_x = 90$ (open circles and squares) were simulated with $\epsilon = 0$ (no inhibition; squares) and $\epsilon/E_a = -10^6$ (with inhibition; circles). $n_s = 10^4$, $\phi = 1/6$, and $x_A = 0.1$.

conducted at a coverage fraction of $\phi = 3/16$, at constant number of particles, by adding an empty row and column to the sides of the unit cell, and qualitatively similar dependence on system size was observed as in $\phi = 1/3$ case. Results equivalent to those obtained using the highly symmetric initial arrangement resulted when each simulation started from a random configuration because the initial condition randomizes by diffusion on shorter times than those needed for noncatalytic reactions.

V. CONCLUDING REMARKS

The rudimentary model presented in this work is capable of simulating chiral symmetry breaking, evidenced by bimodal probability distribution functions of the fraction of a given enantiomer, obtained from unbiased initial conditions. This behavior emerges spontaneously as a result of the subtle interplay of reaction, diffusion, autocatalysis, and inhibition. We are not aware of another model with molecularly explicit chirality, microscopic degrees of freedom, autocatalysis, and inhibition that exhibits symmetry breaking. This suggests a useful role for theory and modeling in elucidating the possible conditions that may have given rise to the emergence of enantiomeric excess in the prebiotic world, as well as for identifying strategies for the rational design of industrial chiral synthesis processes.

A simple rejection kinetic Monte Carlo algorithm was used to simulate the behavior of the model. This algorithm becomes inefficient when reaction acceptance probabilities are low. A rejection-free kinetic Monte Carlo algorithm, described elsewhere,[41] may be used in the future to simulate the infinite-diffusion-rate limit. The model cannot break symmetry in an infinite system with finite diffusion rates because, although arbitrarily many domains with enantiomeric excess will occur in that case, they will cancel each other statistically, and the average enantiomeric excess of the entire system will approach zero in the thermodynamic limit. A simple modification of the model that accounts for reversible reactions and local mass action kinetics could asymptotically lead to symmetry breaking in arbitrarily large systems. Results from this and other enhancements of the present model will be the subject of future publications.

Several extensions of the present simple model may provide further insight into chiral symmetry breaking. The currently irreversible enantiomer-formation reactions can be modified by augmenting them with at least small positive values for their corresponding reverse reaction rates (thereby addressing contention in the literature on the effect of reversibility on symmetry breaking[42,43]), as well as with additional catalytic cluster processes that have dominant enantiomers dissociating their mirror images. Solvent interactions can also be readily incorporated. To simulate the Soai reaction[24] more explicitly, catalyst complexes may also be considered. Incorporation of hydrodynamic effects can provide insight on the role of mixing as a mechanism for the suppression of local fluctuations, and its consequences for the system-size dependence of the appearance of symmetry-breaking conditions. Finally, a three-dimensional extension of the lattice model is feasible with chiral molecules that are represented on a simple cubic lattice by three mutually orthogonal, contiguous line segments in a bent linear pattern, where chirality is distinguished by the sign of the scalar triple product for the bond vectors. The autocatalytic configuration in this three-dimensional extension involves occupancy of all eight vertices of a fundamental cube, which is geometrically possible only by model molecules of the same chirality.

ACKNOWLEDGMENTS

We thank Professor Donna Blackmond for valuable comments on the manuscript and for guidance and helpful discussions concerning this research project. This work was supported by the National Science Foundation (Collaborative Research in Chemistry Grant No. CHE-0908265 to P.G.D.).

[1] M. Bolli, R. Micura, and A. Eschenmoser, Chem. Biol. **4**, 309 (1997).
[2] M. M. Green and B. A. Garetz, Tetrahedron Lett. **25**, 2831 (1984).
[3] I. Budin and J. W. Szostak, Annu. Rev. Biophys. **39**, 245 (2010).
[4] G. F. Joyce, G. M. Visser, C. A. A. van Boeckel, J. H. van Boom, L. E. Orgel, and J. van Westrenen, Nature **310**, 602 (1984).
[5] C. Drahl, Chem. Eng. News **87**, 38 (2009).
[6] S. Pizzarello and M. Lahav, Orig. Life Evol. Biosph. **40**, 1 (2010).
[7] R. Breslow, M. Levine, and Z.-L. Cheng, Orig. Life. Evol. Biosph. **40**, 11 (2010).
[8] S. Toxvaerd, Phys. Rev. Lett. **85**, 4747 (2000).
[9] M. Klussmann, A. J. R. White, A. Armstrong, and D. G. Blackmond, Angew. Chem. Int. Ed. **45**, 7985 (2006).
[10] M. Klussmann, H. Iwamura, S. P. Mathew, D. H. Wells, Jr., U. Pandya, A. Armstrong, and D. G. Blackmond, Nature **441**, 621 (2006).
[11] D. G. Blackmond and M. Klussmann, Chem. Commun. **39**, 3990 (2007).
[12] M. Klussmann, T. Izumi, A. J. P. White, A. Armstrong, and D. G. Blackmond, J. Am. Chem. Soc. **129**, 7657 (2007).
[13] T. G. Lombardo, F. H. Stillinger, and P. G. Debenedetti, Proc. Natl. Acad. Sci. USA **106**, 15131 (2009).
[14] R. Breslow and Z.-L. Cheng, Proc. Natl. Acad. Sci. USA **106**, 9144 (2009).
[15] M. Cao and P. A. Monson, J. Chem. Phys. **112**, 054505 (2005).
[16] C. Viedma, Phys. Rev. Lett. **94**, 065504 (2005).
[17] J. H. E. Cartwright, O. Piro, and I. Tuval, Phys. Rev. Lett. **98**, 165501 (2007).
[18] W. L. Noordiun, T. Izumi, A. Millemaggi, M. Leeman, H. Meekes, W. J. P. van Enckevort, R. M. Kellogg, B. Kaptein, E. Vlieg, and D. G. Blackmond, J. Am. Chem. Soc. **130**, 1158 (2008).
[19] M. Uwaha, J. Phys. Soc. Jpn. **77**, 083802 (2008).
[20] J. McBride and J. Tully, Nature **452**, 161 (2008).
[21] D. G. Blackmond, Chem. Eur. J. **13**, 3290 (2007).
[22] W. L. Noorduin, H. Meekes, A. A. C. Bode, W. J. P. van Enckevort, B. Kaptein, R. M. Kellogg, and E. Vlieg, Cryst. Growth Des. **8**, 1675 (2008).
[23] F. Frank, Biochim. Biophys. Acta **11**, 459 (1953).
[24] K. Soai, T. Shibata, H. Morioka, and K. Choji, Nature **378**, 767 (1995).
[25] T. Shibata, K. Choji, T. Hayase, Y. Aizu, and K. Soai, Chem. Commun. **10**, 1235 (1996).
[26] T. Shibata, H. Morioka, T. Hayase, K. Choji, and K. Soai, J. Am. Chem. Soc. **118**, 471 (1996).
[27] D. G. Blackmond, C. R. McMillan, S. Ramdeehul, A. Schorm, and J. M. Brown, J. Am. Chem. Soc. **123**, 10103 (2001).
[28] D. G. Blackmond, Proc. Natl. Acad. Sci. USA **101**, 5732 (2004).
[29] F. G. Buono and D. G. Blackmond, J. Am. Chem. Soc. **125**, 8978 (2003).
[30] F. G. Buono, H. Iwamura, and D. G. Blackmond, Angew. Chem. Int. Ed. **43**, 2099 (2004).
[31] D. K. Kondepudi and K. Asakura, Acc. Chem. Res. **34**, 946 (2001).
[32] K. Mislow, Collect. Czech. Chem. Comm. **68**, 849 (2003).
[33] Y. Saito and H. Hyuga, J. Phys. Soc. Jpn. **73**, 1685 (2004).
[34] D. Hochberg, and M.-P. Zorzano, Chem. Phys. Lett. **431**, 185 (2006).
[35] D. K. Kondepudi, R. J. Kaufman, and N. Singh, Science **250**, 975 (1990).
[36] D. G. Blackmond, Adv. Synth. Catal. **344**, 156 (2002).

[37] S. K. Teo, W. A. Colburn, W. G. Tracewell, K. A. Kook, D. I. Stirling, M. S. Jaworsky, M. A. Scheffler, S. D. Thomas, and O. L. Laskin, Clin. Pharmacokinet. **43**, 311 (2004).
[38] A. Mannschreck, R. Kiesswetter, and E. von Angerer, J. Chem. Educ. **84**, 2012 (2007).
[39] H. C. Kang and W. H. Weinberg, Acc. Chem. Res. **25**, 253 (1992).
[40] J. F. Kenney, and E. S. Keeping, *Mathematics of Statistics* (D. Van Nostrand Company, New York, 1954), Vol. 1, pp. 100–101.
[41] B. Meng and W. H. Weinberg, J. Chem. Phys. **100**, 5280 (1994).
[42] D. G. Blackmond and O. K. Matar, J. Phys. Chem. B **112**, 5098 (2008).
[43] M. Mauksch and S. B. Tsogoeva, Chem. Phys. Chem. **9**, 2359 (2008).